Rapid Communications

Diffusion-dominated mixing in moderate convergence implosions

A. B. Zylstra,[1,*] N. M. Hoffman,[1] H. W. Herrmann,[1] M. J. Schmitt,[1] Y. H. Kim,[1] K. Meaney,[1] A. Leatherland,[2] S. Gales,[2] C. Forrest,[3] V. Yu. Glebov,[3] M. Schoff,[4] M. Hoppe,[4] and N. Ravelo[4]

[1]*Los Alamos National Laboratory, Los Alamos, New Mexico 87545, USA*

[2]*Plasma Physics Department, AWE plc, Reading RG7 4PR, United Kingdom*

[3]*Laboratory for Laser Energetics, University of Rochester, Rochester, New York 14623, USA*

[4]*General Atomics, San Diego, California 92186, USA*

(Received 1 September 2017; revised manuscript received 18 December 2017; published 14 June 2018)

High-Z material mixed into the fuel degrades inertial fusion implosions and can prevent ignition. Mix is often assumed to be dominated by hydrodynamic instabilities, but we report Omega data, using shells with $\sim$150 nm deuterated layers to gain unprecedented resolution, which give strong evidence that the dominant mix mechanism is diffusion for these moderate temperature ($\lesssim$6 keV) and convergence ($\sim$12) implosions. Small-scale instability-driven or turbulent mix is negligible.

DOI: 10.1103/PhysRevE.97.061201

A burning fusion plasma requires a temperature exceeding the ideal ignition point, and for the product of plasma pressure and energy confinement time ($p\tau$), including all loss mechanisms, to exceed a critical value [1]. Inertial confinement fusion (ICF) seeks to reach these conditions via compression of the fuel by spherical implosion [2]. Radiation drive (laser beams or laser-generated x rays) is incident upon the outer surface of a capsule containing the deuterium-tritium (DT) fuel, generating $\sim$100 Mbar ablation pressures on the outside of the capsule, imploding the fuel. While some self-heating [3] has recently been achieved in implosions at the National Ignition Facility (NIF) [4], ignition remains elusive [5,6].

One key degradation mechanism is "mix" of any material with $Z > 1$ into the fuel, particularly the hot spot, where it can quench self-heating. Mix material is damaging because it both increases the heat capacity of the fuel, reducing the temperature, and increases the bremsstrahlung x-ray emissivity, reducing the energy confinement time. Typically the capsule (ablator) material is plastic, diamond [7], or beryllium [8], and is doped with a mid- or high-Z element as a preheat shield. Mix caused significantly reduced fusion yields for early low-adiabat (α, ratio of fuel pressure to Fermi pressure) experiments [9] at $\alpha \sim 1.5$. Recent experiments at $\alpha \sim 2.5$ have had lower levels of mix [10].

Several physical mechanisms can cause mix. The predominant cause is thought to be growth of initial imperfections in the target by hydrodynamic instabilities such as Rayleigh-Taylor (RT), Richmeyer-Meshkov (RM), or Kelvin-Helmholtz (KH). For RT, growth in the linear phase or evolution into the nonlinear (saturated) phase [11] are important. The outer surface of the capsule (ablation front) is RT unstable during acceleration, and the inner surface is unstable during deceleration. In numerical models, buoyancy-drag turbulence models [12] are often used in lieu of fully resolving the instabilities. Localized defects including the capsule support structure [13,14] and fill tube [15] can cause injection of capsule material into the fuel, and degrade performance [16]. Thirdly, at any interface of two materials, such as the fuel and shell material, plasma diffusion can mix the materials. As these mechanisms have fundamentally different dependences on the implosion design and conditions, it is necessary to understand the importance of each to design an ignition-relevant implosion with acceptably low levels of mix. For example, improving the capsule surface quality will suppress the seeds for hydrodynamic instability, but have negligible impact on localized defect- or diffusion-driven mix.

Mix is commonly diagnosed by measuring the plasma's enhanced broadband x-ray emissivity [9], emission spectra of dopant materials [17], or by the separated fusion reactant technique [18–25], in which the total yield of a reaction where one reactant is initially in the shell and the other is in the fuel is used to quantitatively characterize the amount of mixed material. The growth rate of sinusoidal perturbations can also be measured by radiography [26–28]. Most models of separated-reactant experiments assume that the mix is dominated by instabilities, which are typically approximated by a turbulent mix model (e.g., Ref. [23]). One exception is Ref. [25] which found that very hot (>10 keV) and very low convergence ratio (CR $\sim$ 4; the initial to final radius ratio) implosions had diffusion-dominated mix; since these were shock-dominated implosions lacking a deceleration phase, it was expected that instability-driven mix would be small.

In this Rapid Communication, we present results using the separated-reactant technique using very thin layers of the reactant in the shell. These high-resolution measurements of the effective mix depth provide evidence that gas-filled moderate temperature (<6 keV) and moderate convergence ($\sim$12) direct-drive OMEGA implosions are dominated by diffusive mix during peak nuclear burn, and that any turbulence-driven mix layer is less significant.

These experiments were performed on the OMEGA laser [29]. The 60 laser beams delivered a total of 27 kJ of energy in a 1-ns-duration square pulse. Each beam's illumination profile

*zylstra@lanl.gov

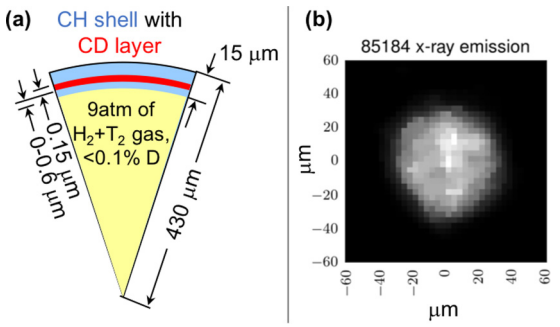

FIG. 1. (a) Radial cross section of the capsules used: 15-μm-thick plastic shells, 860 μm diameter, with a 0.15 μm deuterated layer. The capsules were filled with 9 atm of equimolar H_2 and T_2 gas. (b) Example framing camera image of the stagnated plasma on shot 85184, where the grayscale represents x-ray surface brightness.

was smoothed using SG5 distributed phase plates (DPPs) [30], distributed polarization rotation (DPR) [19], and smoothing by spectral dispersion (SSD) [31]. The incident laser intensity is thus $\sim 10^{15}$ W/cm^2 on the surface of an 860-μm-diameter capsule; approximately 40% of the laser energy is scattered while the rest is absorbed at the critical density, creating ablation pressures on the order of 100 Mbar, imploding the shell. Figure 1(a) shows a capsule schematic. The shell is plastic, predominantly CH (56.9% H, 40.6% C, 2.5% O) with a 0.15-μm-thick deuterated layer (CD) either at the inner surface or recessed by up to 0.6 μm. The capsules are filled with 9 atm of gas, composed of equimolar H_2 and T_2 with a small deuterium impurity ($\lesssim$0.05% atomic). Reference shots used equivalent shells without the deuterated layer and either the same gas fill or gas premixed with 2% atomic deuterium.

The laser drive ablates the outer ~8–9 μm of the shell, with the remaining shell material reaching peak velocity (kinetic energy) at the end of the laser drive. During deceleration the kinetic energy is converted to internal energy in the fuel, which burns for ~100 ps and then disassembles. The plasma's broadband x-ray emission at stagnation is imaged using gated pinhole imaging [32]. An example image from shot 85184 is shown in Fig. 1(b). The camera is filtered with 200 μm of Be and uses 10-μm-diameter pinholes at a magnification of 6×. The emission corresponds to the hot spot, in this case with a radius of ~33 μm, taken from the 20% contour, for a convergence ratio of ~13. On average the shots used in this work had a measured CR = 12 ± 1.

The implosion generates the fusion reactions

$$\mathrm{T} + \mathrm{T} \rightarrow {}^4\mathrm{He} + 2n \ \ (\mathrm{Q} = 11.3\ \mathrm{MeV}), \tag{1}$$

$$\mathrm{D} + \mathrm{T} \rightarrow {}^4\mathrm{He}\ (3.56\ \mathrm{MeV}) + n(14.03\ \mathrm{MeV}). \tag{2}$$

The T + T reaction generates neutrons with a broad energy distribution between zero and 11.3 MeV [33], while the D + T reaction generates a monoenergetic neutron at 14 MeV. The entire neutron spectrum is measured using time-of-flight detectors [34], giving the total yield of each reaction. Since tritium is only present in the initial gaseous fuel, the TT fusion yield represents the "clean" burn of the fuel. A small amount of DT yield results from the fuel's deuterium contamination (~0.05% atomic), so any appreciable amount of DT yield must come from mix of the the CD layer into the fuel.

These types of implosions can be predicted using a radiation-hydrodynamics simulation-based model of these implosions. The model includes reduced laser intensity due to scattered light, artificial preheat of the shell material due to radiation or hot electrons, a turbulent mix model with an adjustable scale length [12], and the Zimmerman-Paquette-Kagan-Zhdanov (ZPKZ) diffusion model [35–38]. The ZPKZ diffusion model incorporates thermodiffusion of multiple ion species, frictional ion heating, and the advective transport of ion enthalpy, in addition to the processes of concentration diffusion, barodiffusion [39], and electrodiffusion, which were the only processes included in an earlier diffusion model described in Ref. [35]. There are no free parameters associated with the ZPKZ model.

This one-dimensional radiation-hydrodynamics simulation model class, incorporating turbulent mix and ion-kinetic multispecies transport, has been successful in explaining many observed features of a wide range of capsule experiments. The first description of our approach, using a reduced kinetic model for fusion reactivity reduction and including comparisons to capsule data, appeared in Molvig *et al.* (Ref. [40]). Another early version, this time including turbulent mix and multispecies ion diffusion, was first applied to analyze DT-filled-plastic-shell OMEGA capsule experiments conducted in 2013 [41]. Figure 3 of that article shows the validity of the simulation model for explaining observed DT yields and burn-averaged ion temperatures, for capsules with shells as thick as 30 μm, and illustrates the effect of the turbulent mix model. In other work, summarized in Ref. [35], the simulation model was successful in explaining hot, thin-shell implosions without the need to invoke a turbulent mix model. This article describes applications of the simulation model to experiments carried out by Rosenberg *et al.* (Ref. [42]) and Rinderknecht *et al.* (Ref. [25]); the latter two articles themselves contain results of our simulation model. Our results were compared to experiments and kinetic simulations by Larroche *et al.* (Ref. [43]), and the simulation model was recently used in an extensive study of prediction under uncertainty by Osthus *et al.* (Ref. [44]).

As a result of the studies described by Kim *et al.* and Hoffman *et al.* (Refs. [41] and [35]), we were led to expect that turbulent mix plays a role for thicker shells, 15 μm and greater, but not for thinner shells. For these experiments we made preshot predictions using the turbulence model, with initial turbulent length scales calibrated to previous separated-reactant experiments. To predict the data trend with CD recession depth before the experiment, the three free parameters of the overall simulation model (absorption, preheat, and turbulent scale length) were inferred from fitting data using shells and drive similar to Fig. 1, with 1-ns-duration square pulse laser drive and 15-μm-thick, 860-μm-diameter plastic shells. Shot 80348 had a 0.3-μm-thick CD layer at the interface, and was filled with 9 atm of equimolar HT gas. Shot 72831 had a 1-μm-thick CD layer recessed by 1 μm, and was filled with 10 atm of pure T_2 gas [45]. This previous work presents an underconstrained problem for the model, but was used for preshot calibration. Our experiment's variation in recession depth was designed to provide a strong constraint on the model.

TABLE I. Tuning data and calculated observables for the two turbulence + diffusion models, plus the inferred parameters.

	Diff.+Turb. no. 1		Diff.+Turb. no. 2	
	80348	Model	72831	Model
Y_{DT} ($\times 10^{12}$)	1.22 ± 0.06	1.25	1.54 ± 0.11	1.60
Y_{HT} ($\times 10^{7}$)	1.9 ± 0.5	1.5		
Y_{TT} ($\times 10^{11}$)			7.90 ± 1.2	6.92
T_i DT (keV)	4.4 ± 0.6	4.2	5.5 ± 0.5	4.3
BT (ns)	1.45 ± 0.05	1.32	1.46 ± 0.05	1.40
BW (ps)	103 ± 14	105	184 ± 25	70
Model parameters				
f_{pre}	0.0225		0.005	
f_{ls}	0.82		0.779	
λ (μm)	0.4		0.511	
Shot parameters				
Capsule				
Radius (μm)	872.2		865	
Thick. (μm)	15.0		15.0	
Laser				
Energy (kJ)	25.8		26.2	
Gas fill	9 atm H_2/T_2		10 atm T_2	
CD layer				
Thick. (μm)	0.3		1.0	
Depth (μm)	0		1.0	

The basic nuclear observables from these two shots are shown in Table I: the yields (Y) of DT, TT, and HT; the DT burn-averaged ion temperature (T_i); the bang time (BT), and the burn width (BW). A χ^2 minimization routine is run to infer the three free parameters in our model: the preheat fraction (f_{pre}), the laser absorption fraction (f_{ls}), and the turbulence scale length (λ). The inferred parameters and the calculated observables for the two reference shots are also shown in Table I. None of the model parameters affect the ZPKZ ion diffusion model.

The nuclear data from this experiment are shown in Fig. 2: the DT neutron yield (a), and the ratio of the DT to TT yield (b) versus the CD layer recession depth. The data are the blue points; recession depths of 0, 0.33, and 0.66 μm were used with two shots at each point. The DT yield (both raw and normalized to TT) is highest when the CD layer is at the interface, and drops approximately two orders of magnitude for the 0.33 and 0.66 μm recession depths. In Fig. 2(b) the horizontal blue dotted line represents the measured DT/TT yield ratio in a CH shell implosion with contaminant D only, and the horizontal blue dashed line is the yield ratio when 2% D is introduced into the gas fill of a CH shell implosion. The mix in the zero recession depth case corresponds to an equivalent of ~4% D premixed, which would require that ~27% of the 150-nm-thick deuterated layer mix into the gas.

The nuclear predictions using the preshot model parameters, described above, are shown in Fig. 2 by the green dashed (Diff.+Turb. no. 1) and green dotted curves (Diff.+Turb. no. 2), respectively. Neither model adequately explains the new data, with a significant underprediction of the experiment at 0

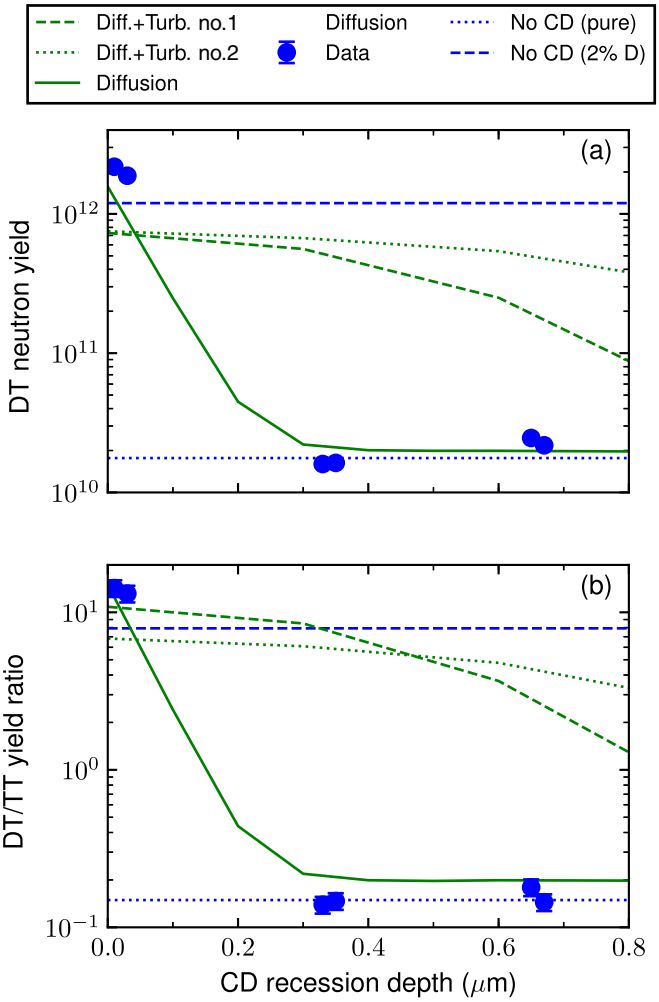

FIG. 2. Nuclear data versus CD recession: DT neutron yield (a), and DT/TT yield ratio (b). Model curves are shown by the green curves. The blue horizontal dashed and dotted lines represent values from 2% D in the gas or contamination D (0.05%). Red circles are individual shots simulated with the diffusion-only model.

recession depth, and significant overprediction as the recession increases. Because the turbulence scale length in these models is of order 1 μm, turbulence transports material from deep in the shell into the fuel, and has a fundamental relationship between the mix depth into the shell and its penetration into the core, similar to the bubble-spike height ratio in RT instability growth.

The data clearly indicate that the mixed deuterium comes from a thin layer immediately adjacent to the interface, with no mix observable above background levels for 0.33 μm recession. This trend can be explained if the mix is purely due to diffusive transport—a model with zero turbulence scale length ($f_{pre} = 0.008$, $f_{ls} = 0.725$, and $\lambda = 0$) is shown by the green solid curve in Fig. 2 and explains the data. Simply decreasing the turbulence scale length cannot reproduce both the 0 and 0.33 μm recession data. A detailed statistical discussion demonstrating the necessity of a zero turbulence scale length is given in the Supplemental Material [46]. The diffusion-only model is also used to perform specific postshot

TABLE II. Data and model results from shots with 0.15- and 0.3-μm-thick CD layers.

	80348		85184	
Thickness (μm)	15.0		14.3	
O.D. (μm)	872		868	
CD (μm)	0.3		0.15	
Laser (kJ)	25.834		26.724	
E/mass (J/μg)	729.3		797.2	
	Data	Model	Data	Model
Y_{DT} ($\times 10^{12}$)	1.22 ± 0.06	1.49	1.88 ± 0.09	1.97

calculations of each shot, including actual target and laser conditions, which are shown by the red circles.

The primary experimental set used in this work had 0.15-μm-thick CD layers recessed in steps of 0.3 μm, so the first shots had deuterated plastic from $0 \rightarrow 0.15$ μm, the second from $0.3 \rightarrow 0.45$ μm, and so on. This data leaves a gap from $0.15 \rightarrow 0.3$ μm, which could have material contributing to the total mix mass. This layer of material can be studied using the older shot, 80348, which had a 0.3-μm-thick layer of CD at the interface, thus spanning $0 \rightarrow 0.3$ μm of depth. When combined with the primary data set, this covers the entire range of the first $\sim 1/2$ μm.

A detailed comparison of shots with 0.15- and 0.3-μm-thick layers at the interface is shown in Table II, including the shot setup parameters: the shell thickness and outer diameter, the CD layer thickness, the total laser energy, and the drive energy per unit mass of the capsule. The measured and modeled DT (mix) yields are also shown.

Due to experimental variability, 85184 had a slightly thinner and smaller shell driven by more laser energy. These variations all go in the direction of a more strongly driven capsule, with ~9% more energy per unit mass. Even though 85184 had a thinner CD layer, this increase in specific drive is enough to increase the overall mix yield by about 50%. This change is captured by the diffusion-only model. In the postshot simulation of 80348, approximately 93% of the mixed deuterium comes from the inner 0.15 μm layer, and ~7% comes from material between 0.15 and 0.3 μm in depth. This result clearly suggests that the material between 0.15 and 0.3 μm depth is not a significant contributor to the overall mix, and corroborates the conclusion from the 0.15-μm-thick layers that the dominant mix mechanism is diffusion.

The differences in transport of shell material into the hot spot between the turbulence and diffusion-only models are shown in Fig. 3. The diffusion-plus-turbulence no. 1 and diffusion-only models are the top and bottom rows, respectively, for simulations where the CD layer is at the interface (left column) or recessed by 0.3 μm (right column). The plots show the normalized ion number fraction versus normalized radius for hydrogen (black), tritium (green), carbon (red), deuterium (blue), and oxygen (magenta). The radius is normalized to the radius of peak shell density at the time of the plot, near bang time, in a simulation using the diffusion-only model, with the same value of the reference radius used for all plots. The combination of turbulence and diffusion creates a large mix layer where both C and D from the shell are effectively mixed

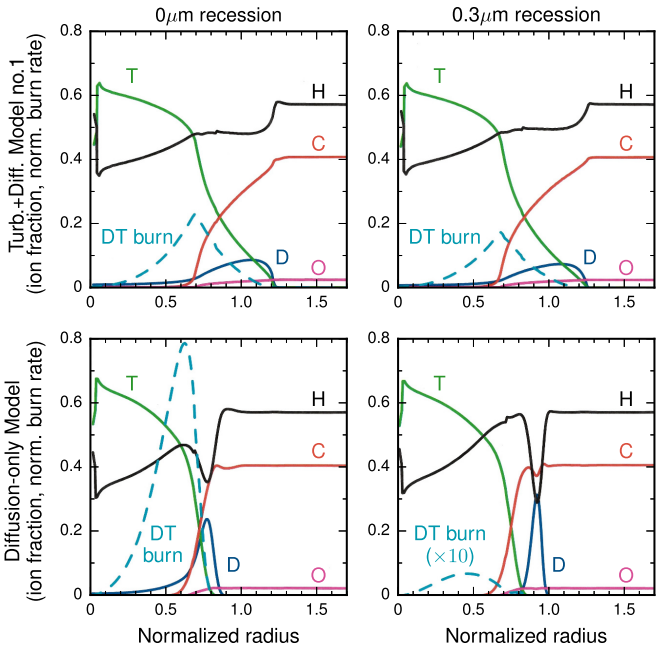

FIG. 3. Ion species number fraction (for H, C, T, D, O) versus normalized radius for the turbulence + diffusion no. 1 model (top row) and diffusion-only model (bottom row) for CD recession depths of 0 μm (left) and 0.3 μm (right). The cyan dashed curve shows the DT reaction rate ($n_D n_T \langle \sigma v \rangle r^2$) versus radius.

with the fuel, and there is very little difference with the 0.3 μm recession, leading to a small difference in predicted yield (see Fig. 2). The effect of diffusion is suppressed with the turbulence model because the gradients, including in the ion-species concentration, are significantly reduced. Further, the diffusion coefficient is affected by the altered plasma conditions, and the long-scale-length turbulence can continuously overtake and suppress any diffusive layer that forms between the mixed layer and the clean fuel. The lower left panel clearly shows the diffusive separation of D from C, an effect which allows significant mix yield from the product $n_D \times n_T$ being large in a region without C, an effect which cannot happen by turbulent mixing. For the 0.3 μm recessed layer the mix layer is smaller than the recession depth, leading to essentially zero mix yield since $n_D \times n_T$ is small or zero at all radii.

The diffusion process is particularly effective at liberating D from the plastic shell and transporting it well into the hotter, less dense fuel since the ion mean free path is significantly longer in the fuel than in the shell. From Kagan and Tang (Ref. [38]), the diffusivity in a binary mixture can be written as

$$D = 747 \frac{T_i^{5/2}}{F_{lh} \rho \ln \Lambda} \sqrt{\frac{1}{A_h} + \frac{1}{A_l}} \frac{\bar{A}}{Z_l^2 Z_h^2} \text{ cm}^2/\text{s}, \qquad (3)$$

where A_l and A_h are ion masses in atomic mass units, and Z_l and Z_h are the ion charges, of the light (l) and heavy (h) species. $\bar{A}$ is the number-weighted mean ion mass, T_i (in keV) is the ion temperature, and ρ (in g/cm^3) is the mass density. F_{lh} is a dynamic friction coefficient, calculated kinetically, with a value generally between 1/3 and 1. For the diffusivity

of deuterium,

$$D = \mathcal{D}\frac{T_i^{5/2}}{F_{lh}\rho}\frac{6}{\ln\Lambda}\ \mu\mathrm{m}^2/\mathrm{ns}, \tag{4}$$

where $\mathcal{D}$ depends on the background plasma: for CD we assume that the carbon dominates the deuterium's diffusivity, so the above equation (with $A_h = 12$, $A_l = 2$, $Z_h = 6$, $Z_l = 1$, and $\bar{A} = 7$) gives $\mathcal{D} = 1.85$. For a 50/50 HT mixture, where the HT is approximated as a single average ion species with $A_h = A_l = 2$ (and $Z_h = Z_l = 1$, $\bar{A} = 2$), $\mathcal{D} = 24.9$. As examples, assuming $F_{lh} = 1$ and $\ln\Lambda = 6$, we find $D_{\mathrm{CD}} = 5.1\ \mu\mathrm{m}^2/\mathrm{ns}$ at 1.5 keV and 1 g/cm^3 (approximate shell conditions), while $D_{\mathrm{HT}} = 1590\ \mu\mathrm{m}^2/\mathrm{ns}$ at 4.0 keV and 0.5 g/cm^3 (fuel conditions near the interface). The diffusivity is substantially higher in the fuel since it is $\propto T_i^{5/2}/\rho Z_h^2$. The deuterium diffusion distance is $\sqrt{D\tau}$ in time τ, so in 100 ps it would diffuse 0.7 μm in CD (shell), but would diffuse 13 μm in HT (fuel). This example illustrates why deuterium can diffusively emerge from a very thin surface layer of plastic and then quickly spread into the fuel. Figure 3 also shows the DT (mix) reaction rate versus radius as the product of the volumetric reactivity ($n_{\mathrm{D}}n_{\mathrm{T}}\langle\sigma v\rangle$) and radius squared. In the turbulence+diffusion model approximately half of the mix yield comes from deuterium that penetrates deep into the fuel, and about half from the large mix layer (normalized radius ~0.7–1.2). Since the diffusion mechanism efficiently injects deuterium into otherwise clean HT fuel (normalized radius $\lesssim 0.7$), the mix (DT) yield in the diffusion simulation is dominated by the tail at relatively smaller radius, which is dramatically suppressed for recessed layers.

These data provide a strong constraint on implosion fuel-shell mix modeling. By using thin layers in a separated-reactant experiment, we find evidence that the dominant mix mechanism for moderate temperature (~6 keV) and convergence (~12) direct-drive implosions on OMEGA is due to ion diffusion across the fuel-shell interface. Unlike low-convergence implosions where the burn is shock dominated [25], hydrodynamic instability at the fuel-shell interface was expected to be significant in these implosions as they undergo a deceleration phase where the dense shell stagnates on the hot spot; during this phase the fuel-shell interface is highly unstable to Rayleigh-Taylor instability. The instability growth and development into a turbulent mix layer may be suppressed by plasma viscosity or magnetic fields [47–49], while diffusion would be insensitive to these effects. Such mechanisms could be explored in two- or three-dimensional simulations with real plasma viscosity and magnetohydrodynamics. In light of these results, it would be worthwhile to revisit recent experiments that were modeled using the turbulent mix model, for example, Ref. [41].

Since mix is a critical degradation mechanism for inertial fusion, understanding the sources of mix is key for the pursuit of ignition. If diffusion dominates certain separated-reactant experiments, those results may not be directly applicable to ignition capsules with a dense fuel layer surrounding the hot spot. Diffusion, if found to be important in ignition experiments, may be substantially mitigated by increasing the system size or changing plasma conditions at the interface.

We thank the operations crews and engineering staff at OMEGA for supporting these experiments. A.B.Z. gratefully acknowledges the support provided for this work by the Laboratory Directed Research and Development (LDRD) program, Project No. 20150717PRD2, at Los Alamos National Laboratory. This work was performed under the auspices of the U.S. DOE by LANL under Contract No. DE-AC52-06NA52396, and by GA under Contract No. DE-NA0001808.

[1] J. D. Lawson, Proc. Phys. Soc., London, Sect. B **70**, 6 (1957).
[2] J. Nuckolls, L. Wood, A. Thiessen, and G. Zimmerman, Nature (London) **239**, 139 (1972).
[3] O. Hurricane *et al.*, Nature (London) **506**, 343 (2014).
[4] G. Miller, E. Moses, and C. Wuest, Nucl. Fusion **44**, S228 (2004).
[5] M. Edwards *et al.*, Phys. Plasmas **20**, 070501 (2013).
[6] J. D. Lindl *et al.*, Phys. Plasmas **21**, 129902 (2014).
[7] L. F. Berzak Hopkins *et al.*, Phys. Rev. Lett. **114**, 175001 (2015).
[8] J. L. Kline *et al.*, Phys. Plasmas **23**, 056310 (2016).
[9] T. Ma *et al.*, Phys. Rev. Lett. **111**, 085004 (2013).
[10] T. Ma *et al.*, Phys. Plasmas **24**, 056311 (2017).
[11] S. W. Haan, Phys. Rev. A **39**, 5812 (1989).
[12] G. Dimonte, Phys. Plasmas **7**, 2255 (2000).
[13] S. R. Nagel *et al.*, Phys. Plasmas **22**, 022704 (2015).
[14] R. Tommasini *et al.*, Phys. Plasmas **22**, 056315 (2015).
[15] A. G. MacPhee *et al.*, Phys. Rev. E **95**, 031204 (2017).
[16] C. R. Weber *et al.*, Phys. Plasmas **24**, 056302 (2017).
[17] S. P. Regan *et al.*, Phys. Rev. Lett. **111**, 045001 (2013).
[18] R. E. Chrien, N. M. Hoffman, J. D. Colvin, C. J. Keane, O. L. Landen, and B. A. Hammel, Phys. Plasmas **5**, 768 (1998).
[19] D. D. Meyerhofer *et al.*, Phys. Plasmas **8**, 2251 (2001).
[20] C. K. Li *et al.*, Phys. Rev. Lett. **89**, 165002 (2002).
[21] J. R. Rygg, J. A. Frenje, C. K. Li, F. H. Seguin, R. D. Petrasso, V. Yu. Glebov, D. D. Meyerhofer, T. C. Sangster, and C. Stoeckl, Phys. Rev. Lett. **98**, 215002 (2007).
[22] D. C. Wilson, P. S. Ebey, T. C. Sangster, W. T. Shmayda, V. Y. Glebov, and R. A. Lerche, Phys. Plasmas **18**, 112707 (2011).
[23] V. A. Smalyuk *et al.*, Phys. Rev. Lett. **112**, 025002 (2014).
[24] D. T. Casey *et al.*, Phys. Plasmas **21**, 092705 (2014).
[25] H. G. Rinderknecht *et al.*, Phys. Rev. Lett. **112**, 135001 (2014).
[26] V. A. Smalyuk *et al.*, Phys. Rev. Lett. **112**, 185003 (2014).
[27] C. R. Weber *et al.*, Phys. Rev. Lett. **117**, 075002 (2016).
[28] L. A. Pickworth *et al.*, Phys. Rev. Lett. **117**, 035001 (2016).
[29] T. Boehly, D. Brown, R. Craxton *et al.*, Opt. Commun. **133**, 495 (1997).
[30] Y. Lin, G. N. Lawrence, and T. J. Kessler, Opt. Lett. **21**, 1703 (1996).
[31] S. Skupsky, R. W. Short, T. Kessler, R. S. Craxton, S. Letzring, and J. M. Soures, J. Appl. Phys. **66**, 3456 (1989).
[32] D. Bradley, P. Bell, J. Kilkenny, R. Hanks, O. Landen, P. Jaanimagi, P. McKenty, and C. Verdon, Rev. Sci. Instrum. **63**, 4813 (1992).

[33] D. B. Sayre *et al.*, Phys. Rev. Lett. **111**, 052501 (2013).
[34] C. Forrest *et al.*, Rev. Sci. Instrum. **83**, 10D919 (2012).
[35] N. M. Hoffman, G. B. Zimmerman *et al.*, Phys. Plasmas **22**, 052707 (2015).
[36] C. Paquette, C. Pelletier, G. Fontaine, and G. Michaud, Astrophys. J., Suppl. Ser. **61**, 177 (1986).
[37] V. M. Zhdanov, Plasma Phys. Controlled Fusion **44**, 2283 (2002).
[38] G. Kagan and X.-Z. Tang, Phys. Lett. A **378**, 1531 (2014).
[39] P. Amendt, O. L. Landen, H. F. Robey, C. K. Li, and R. D. Petrasso, Phys. Rev. Lett. **105**, 115005 (2010).
[40] K. Molvig, N. M. Hoffman, B. J. Albright, E. M. Nelson, and R. B. Webster, Phys. Rev. Lett. **109**, 095001 (2012).
[41] Y. H. Kim *et al.*, J. Phys.: Conf. Series **717**, 012030 (2016).
[42] M. J. Rosenberg *et al.*, Phys. Rev. Lett. **112**, 185001 (2014).
[43] O. Larroche *et al.*, Phys. Plasmas **23**, 012701 (2016).
[44] D. Osthus, S. Van der Wiel, N. Hoffman, and F. Wysocki (unpublished).
[45] B. M. Haines *et al.*, Phys. Plasmas **23**, 072709 (2016).
[46] See Supplemental Material at http://link.aps.org/supplemental/10.1103/PhysRevE.97.061201 for details of a statistical likelihood analysis of the model parameters, and discussion of other mechanisms.
[47] H. F. Robey, Phys. Plasmas **11**, 4123 (2004).
[48] C. R. Weber, D. S. Clark, A. W. Cook, L. E. Busby, and H. F. Robey, Phys. Rev. E **89**, 053106 (2014).
[49] B. Srinivasan and X.-Z. Tang, Europhys. Lett. **107**, 65001 (2014).